

Gain-enhanced high- k transmission through metal-semiconductor hyperbolic metamaterials

Joseph S. T. Smalley,^{1,2,*} Felipe Vallini,¹ Shiva Shahin,¹ Boubacar Kanté,¹ and Yeshaiahu Fainman¹

¹*Department of Electrical and Computer Engineering, University of California San Diego, La Jolla, CA 92103, USA*

²*Center for Integrated Nanotechnologies, Sandia National Laboratory, Albuquerque, NM 87185, USA*

[*jsmalley@ucsd.edu](mailto:jsmalley@ucsd.edu)

Abstract: We analyze the steady-state transmission of high-momentum (high- k) electromagnetic waves through metal-semiconductor multilayer systems with loss and gain in the near-infrared (NIR). Using a semi-classical optical gain model in conjunction with the scattering matrix method (SMM), we study indium gallium arsenide phosphide (InGaAsP) quantum wells as the active semiconductor, in combination with the metals, aluminum-doped zinc oxide (AZO) and silver (Ag). Under moderate external pumping levels, we find that NIR transmission through Ag/InGaAsP systems may be enhanced by several orders of magnitude relative to the unpumped case, over a large angular and frequency bandwidth. Conversely, transmission enhancement through AZO/InGaAsP systems is orders of magnitude smaller, and has a strong frequency dependence. We discuss the relative importance of Purcell enhancement on our results and validate analytical calculations based on the SMM with numerical finite-difference time domain simulations.

© 2015 Optical Society of America

OCIS codes: (160.3918) Metamaterials; (160.4236) Nanomaterials; (310.6628) Subwavelength structures, nanostructures; (350.4238) Nanophotonics and photonic crystals; (160.3900) Metals.

References and links

1. H. Raether, *Surface Plasmons on Smooth and Rough Surfaces and on Gratings* (Springer Verlag, 1988).
2. J. Schilling, "Uniaxial metallo-dielectric metamaterials with scalar positive permeability," *Phys. Rev. E* **74**, 046618 (2006).
3. I. Avrutsky, I. Salakhutdinov, J. Elser, and V. Podolskiy, "Highly confined optical modes in nanoscale metal-dielectric multilayers," *Phys. Rev. B* **75**, 241402 (2007).
4. S. Zhukovsky, O. Kidwai, and J. Sipe, "Physical nature of volume plasmon polaritons in hyperbolic metamaterials," *Opt. Express* **21**, 14982–14987 (2013).
5. B. Wood, J. Pendry, and D. Tsai, "Directed sub-wavelength imaging using a layered metal-dielectric system," *Phys. Rev. B* **74**, 115116 (2006).
6. Z. Jacob, L. Alekseyev, and E. Narimanov, "Optical hyperlens: Far-field imaging beyond the diffraction limit," *Opt. Express* **14**, 8247–8256 (2006).
7. X. Zhang and Z. Liu, "Superlenses to overcome the diffraction limit," *Nature Materials* **7**, 435–441 (2008).
8. J. Homola, S. Yee, and G. Gauglitz, "Surface plasmon resonance sensors: review," *Sensors and Actuators B: Chemical* **54**, 3–15 (1999).
9. J. Anker, W. Hall, O. Lyandes, N. Shah, J. Zhao, and R. V. Duyne, "Biosensing with plasmonic nanosensors," *Nature Mat.* **7**, 442–453 (2008).

10. T. Xu and H. Lezec, "Visible-frequency asymmetric transmission devices incorporating a hyperbolic metamaterial," *Nature Comm.* **5**, 4141 (2014).
11. C. Duncan, L. Perret, S. Palomba, M. Lapine, B. Kuhlmeier, and C. de Sterke, "New avenues for phase matching in nonlinear hyperbolic metamaterials," *Sci. Rep.* **5**, 8983 (2015).
12. D. Lu, J. Kan, E. Fullerton, and Z. Liu, "Enhancing spontaneous emission rates of molecules using nanopatterned multilayer hyperbolic metamaterials," *Nature Nano.* **9**, 48–53 (2014).
13. K. Sreekanth, K. Krishna, A. D. Luca, and G. Strangi, "Large spontaneous emission rate enhancement in grating coupled hyperbolic metamaterials," *Sci. Rep.* **4**, 6340 (2014).
14. T. Galfsky, H. Krishnamoorthy, W. Newman, E. Narimanov, Z. Jacob, and V. Menon, "Active hyperbolic metamaterials: enhanced spontaneous emission and light extraction," *Optica* **2**, 62–65 (2015).
15. W. Barnes, "Surface plasmon-polariton length scales: a route to sub-wavelength optics," *J. Opt. A: Pure Appl. Opt.* **8**, S87–S93 (2006).
16. S. Maier, *Plasmonics: Fundamental and Applications* (Springer, 2007).
17. I. D. Leon and P. Berini, "Amplification and lasing with surface plasmon-polaritons," in *Plasmonics and Plasmonic Metamaterials*, (World Scientific, 2012), pp. 101–122.
18. M. Noginov, "Metamaterials with optical gain," in *Tutorials in Metamaterials*, (CRC, 2012), pp. 129–161.
19. S. A. Ramakrishna and J. B. Pendry, "Removal of absorption and increase in resolution in a near-field lens via optical gain," *Phys. Rev. B* **67**, 201101(R) (2003).
20. X. Ni, S. Ishii, M. Thoreson, V. Shalaev, S. Han, S. Lee, and A. Kildishev, "Loss-compensated and active hyperbolic metamaterials," *Opt Express* **19**, 25242–25254 (2011).
21. C. Arypropoulos, N. Estakhri, F. Monticone, and A. Alu, "Negative refraction, gain, and nonlinear effects in hyperbolic metamaterials," *Opt. Express* **21**, 15037–15047 (2013).
22. R. S. Savelev, I. V. Shadrivov, P. A. Belov, N. N. Rosanov, S. V. Fedorov, A. A. Sukhorukov, and Y. S. Kivshar, "Loss compensation in metal-dielectric layered metamaterials," *Phys. Rev. B*, **87**, 115139 (2013).
23. S. Zhang, W. Fan, N. Panoiu, K. Malloy, R. Osgood, and S. Brueck, "Optical negative-index bulk metamaterials consisting of 2D perforated metal-dielectric stacks," *Opt. Express* **14**, 6778–6787 (2006).
24. J. Valentine, S. Zhang, T. Zentgraf, E. Ulin-Avila, D. Genov, G. Bartal, and X. Zhang, "Three-dimensional optical metamaterial with a negative refractive index," *Nature* **455**, 376–379 (2008).
25. S. Xiao, V. Drachev, A. Kildishev, X. Ni, U. Chettiar, H. Yuan, and V. Shalaev, "Loss-free and active optical negative-index metamaterials," *Nature* **466**, 735–738 (2010).
26. J. Seidel, S. Grafstrom, and L. Eng, "Stimulated emission of surface plasmons at the interface between a silver film and an optically pumped dye solution," *Phys. Rev. Lett.* **94**, 177401 (2005).
27. I. D. Leon and P. Berini, "Amplification of long-range surface plasmons by a dipolar gain medium," *Nature Photon.* **4**, 382–387 (2010).
28. J. Khurgin and G. Sun, "Practicality of compensating the loss in the plasmonic waveguides using semiconductor gain medium," *Appl. Phys. Lett.* **100**, 011105 (2012).
29. M. Nezhad, K. Tetz, and Y. Fainman, "Gain assisted propagation of surface plasmon polaritons on planar metallic waveguides," *Opt. Express* **12**, 4072–4079 (2004).
30. M. Hill, Y. Oei, B. Smalbrugge, Y. Zhu, T. de Vries, P. van Veldhoven, F. van Otten, T. Eijkemans, J. Turkiewicz, H. de Waardt, E. Geluk, S. Kwon, Y. Lee, R. Notzel, and M. Smit, "Lasing in metallic-coated nanocavities," *Nature Photon.* **1**, 589–594 (2007).
31. K. Ding, Z. C. Liu, M. T. Hill, M. J. H. Marell, P. J. van Veldoven, R. Noetzel, and C. Z. Ning, "Room-temperature continuous wave lasing in deep-subwavelength metallic cavities under electrical injection," *Phys. Rev. B* **85**, 041301 (2012).
32. M. Khajavikhan, A. Simic, M. Katz, J. Lee, B. Slutsky, A. Mizrahi, and Y. Fainman, "Thresholdless nanoscale coaxial lasers," *Nature* **482**, 204–207 (2012).
33. J. S. T. Smalley, F. Vallini, B. Kante, and Y. Fainman, "Modal amplification in active waveguides with hyperbolic dispersion at telecommunication frequencies," *Opt. Express* **22**, 21088–21105 (2014).
34. F. Krayzel, R. Polles, A. Moreau, M. Mihailovic, and G. Granet, "Simulation and analysis of exotic non-specular phenomena," *J Europ Opt Soc* **5**, 10025 (2010).
35. G. Naik, J. Liu, A. Kildishev, V. Shalaev, and A. Boltasseva, "Demonstration of Al:ZnO as a plasmonic component for near-infrared metamaterials," *Proc. Nat. Acad. Sci.* 1121517109 (2011).
36. G. Naik, V. Shalaev, and A. Boltasseva, "Alternative plasmonic materials: Beyond gold and silver," *Adv. Mat.* **25**, 3264–3294 (2013).
37. C. Riley, T. Kieu, J. S. T. Smalley, S. Pan, S. Kim, K. Post, A. Kargar, D. Basov, X. Pan, Y. Fainman, D. Wang, and D. Sirbuly, "Plasmonic tuning of aluminum doped zinc oxide nanostructures by atomic layer deposition," *Phys. Stat. Sol. RRL* **8**, 948–952 (2014).
38. P. Johnson and R. Christy, "Optical constants of noble metals," *Phys. Rev. B* **6**, 4370 (1972).
39. M. Nezhad, A. Simic, O. Bondarenko, B. Slutsky, A. Mizrahi, L. Feng, V. Lomakin, and Y. Fainman, "Room-temperature subwavelength metallo-dielectric lasers," *Nature Photon.* **4**, 395–399 (2010).
40. L. Coldren, S. Corzine, and M. Masanovic, "Gain and current relations," in *Diode Lasers and Photonic Integrated Circuits*, (Wiley, 2012), pp. 157–246.

41. A. Goldberg Yu and N. Schmidt, *Handbook Series on Semiconductor Parameters*, Vol. 2, (World Scientific, 1999).
42. R. Nicholas, J. Portal, C. Houlbert, P. Perrier, and T. Pearsall, "An experimental determination of the effective masses for $\text{Ga}_x\text{In}_{1-x}\text{As}_y\text{P}_{1-y}$ alloys grown on InP," *Appl. Phys. Lett.* **34**, 492–494 (1979).
43. C. Hermann and C. Weisbuch, *Modern Problems in Condensed Matter Sciences*, Vol. 8, (North-Holland, 1984).
44. J. S. T. Smalley, Q. Gu, and Y. Fainman, "Temperature dependence of the spontaneous emission factor in sub-wavelength semiconductor lasers," *IEEE J. Quantum Electron.* **50**, 175–185 (2014).
45. R. Savelev, I. Shadrivov, and Y. Kivshar, "Wave scattering by metal-dielectric multilayer structures with gain," *J. Exp. Theor. Phys. Lett.* **100**, 831–836 (2014).
46. D. Y. K. Ko and J. C. Inkson, "Matrix method for tunneling in heterostructures: Resonant tunneling in multilayer systems," *Phys. Rev. B* **38**, 9945–9951 (1988).
47. D. Y. K. Ko and J. Sambles, "Scattering matrix method for propagation of radiation in stratified media: attenuated total reflection studies of liquid crystals," *J. Opt. Soc. Am. A*, **5** 1863–1866 (1988).
48. T. Visser and H. Blok, "Modal analysis of a planar waveguide with gain and loss," *IEEE J. Quantum Electron.* **31**, 1803–1810 (1995).
49. K. Sreekanth, A. De Luca, and G. Strangi, "Experimental demonstration of surface and bulk plasmon polaritons in hypergratings," *Sci. Rep.* **3**, 3291 (2013).
50. K. Sreekanth, A. De Luca, and G. Strangi, "Excitation of volume plasmon polaritons in metal-dielectric metamaterials using 1D and 2D diffraction gratings," *J. Opt.* **16**, 105103 (2014).
51. A. Yariv and P. Yeh, "Wave propagation in periodic media," in *Photonics: Optical Electronics in Modern Communications* (Oxford, 2007), pp. 539–601.
52. C. Cortes, W. Newman, S. Molesky, and Z. Jacob, "Quantum nanophotonics using hyperbolic metamaterials," *J. Opt.* **14**, 063001 (2012).
53. S. Wuestner, A. Pusch, K. Tsakmakidis, J. Hamm, and O. Hess, "Gain and plasmon dynamics in active negative-index metamaterials," *Phil. Trans. Royal Soc. A* **369**, 3525–3550 (2011).
54. G. Slavcheva, J. Arnold, and R. Ziolkowski, "FDTD simulation of the nonlinear gain dynamics in active optical waveguides and semiconductor microcavities," *IEEE. J. Sel. Top. Quantum Electron.* **10**, 1052–1062 (2004).
55. S. Chang and A. Taflove, "Finite-difference time-domain model of lasing action in a four-level two-electron atomic system," *Opt. Express* **12**, 3827–3843 (2004).
56. L. Ferrari, D. Lu, D. Lepage, and Z. Liu, "Enhanced spontaneous emission inside hyperbolic metamaterials," *Opt. Express* **22**, 4301–4306 (2014).
57. A. Orlov, I. Iorsh, P. Belov, and Y. Kivshar, "Complex band structure of nanostructured metal-dielectric metamaterials," *Opt. Express* **21**, 1593–1598 (2013).
58. S. G. Tikhodeev, A. L. Yablonski, E. A. Muljarov, N. A. Gippius, and T. Ishihara, "Quasiguided modes and optical properties of photonic crystal slabs," *Phys. Rev. B* **66**, 045102 (2002).
59. N. Cotter, T. Presit, and J. Sambles, "Scattering-matrix approach to multilayer diffraction," *J. Opt. Soc. Am. A* **12**, 1097–1103 (1995).
60. S. Gedney and B. Zhao, "An auxiliary differential equation formulation for the complex-frequency shifted PML," *IEEE Trans. Antennas Propag.* **58**, 838–847 (2010).
61. H. Hagenvik, "FDTD simulations of novel gain media," *Thesis*, Norwegian University of Science and Technology (2014).

1. Introduction

Metal-dielectric (MD) interfaces support optical surface waves whose effective wavelength is less than the smallest wavelength achievable in dielectrics [1]. The coupling of multiple MD interfaces enables even smaller effective wavelengths, or conversely higher effective indices, or so-called high- k propagation, of the optical waves [2–4]. The phenomenon of large effective indices and propagating high- k modes lies at the heart of sub-diffraction-limited imaging devices [5–7], sensors based on plasmonic resonances [8, 9], as well as applications of hyperbolic metamaterials (HMMs), including asymmetric transmission devices [10], nonlinear optics [11], and lifetime reduction of dye molecules [12, 13] and quantum dots [14]. Inherent to the increase in the effective index in MD systems, is a concomitant increase in dissipation losses [15, 16]. The tradeoff between optical confinement and losses is a hallmark of plasmonic and hyperbolic media, and may be considered one of the greatest challenges to the widespread realization of integrated plasmonic technology [17, 18].

Strategies for reducing losses in plasmonic and hyperbolic metamaterials have therefore been proposed, including clever design of passive structures and incorporation of active, i.e. gain

media [19–22]. An exemplary case of the former strategy is the fishnet metamaterial [23, 24], whereby air voids in an otherwise continuous MD multilayer open new channels for optical transmission. Even in these structures though, gain media are still necessary to obtain low-loss transmission at optical frequencies, as was demonstrated via infiltrated optical dyes in the core of the structure [25].

While dye molecules are straightforward to model as non-interacting two-level systems and convenient for proof-of-concept experiments [25–27], an ideal gain media in plasmonic systems would be electronically addressable [28]. In this case, semiconductor heterostructures become strong candidates for incorporation into plasmonic systems. III-V semiconductors emitting in the near-infrared (NIR) have been studied in conjunction with surface plasmon amplification [29], and successfully implemented in sub-wavelength metal-coated and plasmonic sources [30–32]. However, the incorporation of active III-V materials in multilayer MD systems with hyperbolic dispersion remains to be demonstrated in the NIR.

In this work, we go beyond effective medium theory [33], and apply the scattering matrix method [34] (SMM) to analyze the possibility for using indium gallium arsenide phosphide (InGaAsP) multiple quantum wells (MQWs) as a gain media in NIR MD systems. InGaAsP is a mature quaternary III-V compound that is epitaxially grown on indium phosphide (InP) substrates. This immediately poses challenges for its incorporation in a multilayer MD system. We envision deposition of metallic thin films into finely patterned trenches between InGaAsP pillars formed by nanoimprint lithography and subsequent reactive ion etching. We assume that the smallest layer thicknesses enabled by this process are 30nm. The resulting MD system, shown schematically in Fig. 1, supports volume plasmon polaritons [4] (VPPs) with large effective indices and large loss in the absence of external pumping, the hallmark of strongly coupled MD interfaces. These high- k VPPs propagate normal to the epitaxial growth direction, which is a novel multilayer configuration, potentially more suitable to waveguide-integrated HMMs, compared to the more common large-area multilayers which are conformal to the wafer substrate. In the following, we show that under moderate external pumping conditions, MD systems composed of InGaAsP MQWs may support transmission of high-index modes enhanced by several orders of magnitude, relative to the unpumped case.

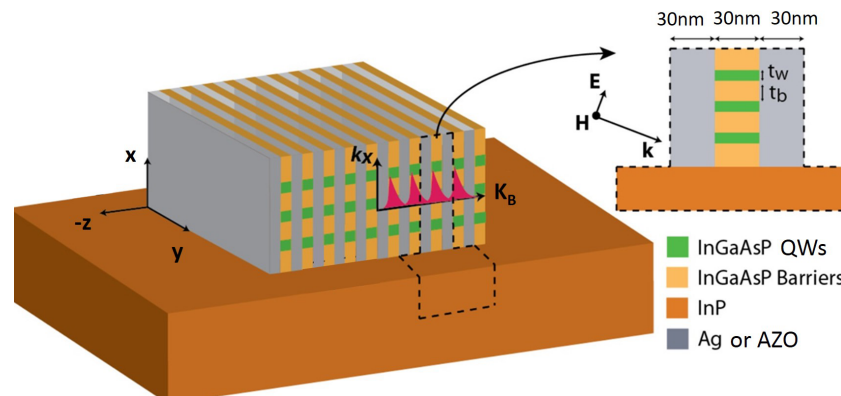


Fig. 1. Schematic of multilayer metal-InGaAsP MQW system. The heterostructure, with $t_{well}=10\text{nm}$ and $t_{barrier}=20\text{nm}$ is grown in the x -direction and TM-polarized light propagates in the z -direction.

In Section 2, we introduce the optical gain model employed, in conjunction with the SMM. We present the main results of the report in Section 3, namely, the NIR transmission char-

acteristics of multilayer MD systems based on InGaAsP MQWs. We investigate InGaAsP in combination with aluminum-doped zinc oxide (AZO), which is considered a low-loss transparent conducting oxide and alternative plasmonic material for NIR applications [35–37], and in combination with silver, which is well known as the noble metal with highest conductivity [38]. In Section 4, we discuss the relative importance of Purcell enhancement on our results. We also validate the analytical SMM results with numerical finite-difference time-domain (FDTD) simulations. We then discuss the limitations of our results, as well as potential extensions. We conclude the report in Section 5.

2. Methods

The quaternary III-V compound that we consider is an $\text{In}_x\text{Ga}_{1-x}\text{As}_y\text{P}_{1-y}$ MQW system where $(x=0.564, y=0.933)$ and $(x=0.737, y=0.569)$ for the wells and barriers, respectively. The nominal room-temperature bandgap energies of the barrier and well materials are 0.953eV ($\lambda_G=1.3\mu\text{m}$) and 0.774eV ($\lambda_G=1.6\mu\text{m}$), respectively. This system can be epitaxially grown on an InP substrate and has been experimentally utilized in near-infrared subwavelength semiconductor lasers [32, 39].

In the dipole-approximation the peak magnitude of the optical gain is governed by the transition matrix element, M_T . Because MD multilayers only support propagation of TM-polarized modes [3], we consider TM-polarized light emission from the quantum wells. To justify the use of a steady-state analysis and the non-inclusion of dynamic nonlinear effects, and for simplicity, we concern ourselves with moderate pumping levels, about two times above the transparency inversion density. Consequently, we may assume that most of the transitions occur at the band-edge such that recombination between electrons and holes with vanishing transverse momentum dominates [40]. In this limit, only transitions from the conduction band to the light-hole band contribute to the matrix element for TM-polarization [40]. We approximate the bandstructure of InGaAsP with parabolic conduction and valence bands, characterized by the conduction and light-hole effective masses of $0.0481m_0$ and $0.0537m_0$, respectively [41], where $m_0=9.1\times 10^{-31}\text{kg}$ is the free electron mass. The magnitude of the matrix element used is given by [42, 43] $|M_T|^2=(24.9\text{eV})m_0/3$, which corresponds to a dipole length of $|x|\approx 2.8\text{nm}$ at $\lambda_0=1500\text{nm}$.

Employing this gain model we obtain complex permittivity values for a 10nm InGaAsP QW at carrier densities representative of absorbing (Abs) and moderately inverted (Inv) states, $N=1.0\times 16\text{cm}^{-3}$ and $N=5.0\times 18\text{cm}^{-3}$, respectively. At $\lambda_0=1500\text{nm}$, the imaginary parts of these values are $\epsilon_{D,Abs}''=\Gamma g(N=1.0\times 16\text{cm}^{-3})=+0.139$ and $\epsilon_{D,Inv}''=\Gamma g(N=5.0\times 18\text{cm}^{-3})=-0.143$, where $\Gamma=1/3$ is the relative area of wells in the InGaAsP heterostructure. Using Kramers-Kronig relations, the real parts at $\lambda_0=1500\text{nm}$ are $\epsilon'_{D,Abs}=11.997$ and $\epsilon'_{D,Inv}=11.881$, respectively. For the sake of simplicity, we used a carrier-independent but frequency dependent real permittivity, which is $\epsilon'_D=11.914$ at $\lambda_0=1500\text{nm}$, and justified because the transmission properties studied are dominated by loss and gain. Relating the imaginary permittivity to the linear gain coefficient [30], $g=-k_0\epsilon_D''(\epsilon'_D)^{-1/2}$, the value of $\epsilon_D''=\pm 0.14$ corresponds to a loss/gain per unit length of $\pm 1700\text{cm}^{-1}$ at 1500nm. The transparency (Tra) condition [40], $\epsilon_{D,Tra}''=0$, for InGaAsP at $\lambda_0=1500\text{nm}$ corresponds to about $N=2.0\times 18\text{cm}^{-3}$. The complex permittivity values for AZO [36] and Ag [38] at $\lambda_0=1500\text{nm}$ are $-0.392+i0.139$ and $-122.190+i3.115$, respectively. Additional details on the gain model may be found in the references [40, 44].

Combined with the presented optical gain model, we use the SMM as implemented by Krayzel et al. [34] to study the transmission properties of an idealization of the structure of Fig. 1. In comparison to simpler methods such as effective medium theory [33], Bloch's theorem [22], and the transfer matrix method [20, 21, 45], the SMM is well known as a superior method for analyzing systems with evanescent waves [46, 47] and strong loss/gain [48]. The ide-

alized structure includes loss and gain, is infinite in the transverse (x - y) plane and surrounded by a uniform medium in the longitudinal (z) direction. To couple to the high- k modes supported by the MD multilayer of Fig. 1, the surrounding medium takes the form of a prism. The prism behaves as a numerical simplification to the physically equivalent grating-coupling technique [10, 12, 14, 49, 50], which is required for practical excitation of the high- k modes supported by each system.

To determine a suitable value of the prism permittivity, ϵ_p , we first determine the bounds of the high- k transmission windows in each MD system. This is achieved using Bloch's theorem [51] in the absence of losses by locating the regions in momentum space wherein the real part of the Bloch vector is purely real. For MD systems with 30nm layer thicknesses and $\lambda_0=1500\text{nm}$, Fig. 2(a) and 2(b) show the real (solid blue curve) and imaginary (dotted blue curve) parts of the Bloch vector, indicating that transmission windows exist when $0 \leq k_x \leq 2.83k_0$ and $4.91k_0 \leq k_x \leq 6.56k_0$ in AZO/InGaAsP and Ag/InGaAsP systems, respectively. In the limit of effective medium theory (dashed red curves), Fig. 2(a) and 2(b) are representative of type-I and type-II HMMs, respectively. Based on these high- k windows, we set $\epsilon_p=64$ for the SMM calculations.

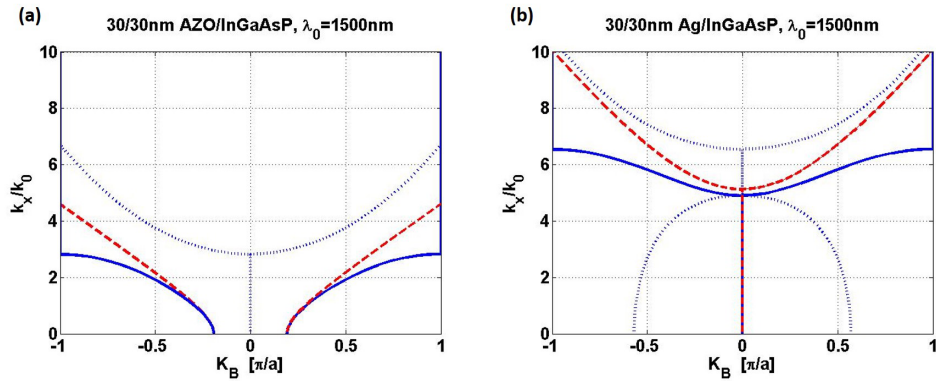


Fig. 2. Wave-vector diagrams for 30/30nm (a) AZO/InGaAsP and (b) Ag/InGaAsP systems at 1500nm with losses omitted. (solid blue line=real part of Bloch vector, dotted blue line=imaginary part of Bloch vector, dashed red line=effective medium theory prediction of real part of Bloch vector) The transmission windows in (a) and (b) extend from $0 \leq k_x \leq 2.83k_0$ and $4.91k_0 \leq k_x \leq 6.56k_0$, respectively.

3. Results

Transmission and reflection at $\lambda_0=1500\text{nm}$ through a 10-period AZO/InGaAsP structure with 30nm layer thicknesses, is shown as a function of incident angle in Fig. 3(a) and 3(b), respectively. The resonances extending from normal incidence to $\theta_{inc}=20^\circ$ translate into a high- k window that extends to roughly $k_x=8\sin(20^\circ) \approx 2.8k_0$, consistent with the prediction based on Bloch's theorem of Fig. 2(a). The effect of inverting the carrier population in absolute terms appears most pronounced near normal incidence and becomes weaker as the incident angle increases. The strong absorption in this system is apparent in the local reflection minimum around $\theta_{inc}=7.5^\circ$. The lack of corresponding transmission maximum indicates strong dissipation, even when the semiconductor is inverted.

Transmission and reflection through the AZO/InGaAsP system is best appreciated when contrasted to the behavior of the Ag/InGaAsP system. In Fig. 3(c) and 3(d), transmission and reflection for the latter system are shown, with identical conditions to the AZO-based structure. The transmission window spans approximately 38.5° to 54.5° , or about $5.0k_0 \leq k_x \leq 6.5k_0$, again

consistent with Bloch's theorem of Fig. 2(b). The effect of inverting the carrier population becomes dramatic in both absolute and relative terms. For several resonances between 39° and 47° , or between $5.0k_0$ and $5.7k_0$, the transmission and reflection exceed unity, indicating active behavior of the system.

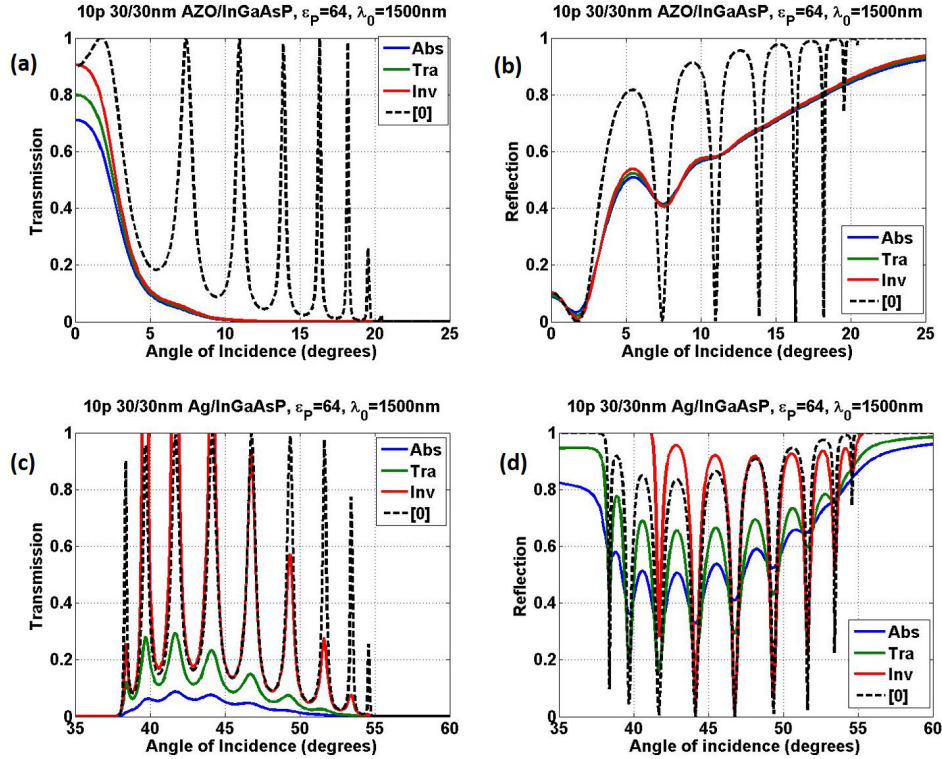


Fig. 3. (a,c) Transmission and (b,d) reflection for TM-polarized light of wavelength 1500nm, incident on 10-period (a,b) AZO/InGaAsP and (c,d) Ag/InGaAsP multilayer with 30nm layers, coupled via prism with $\epsilon_p=64$. (Abs: $N=1 \times 10^{16} \text{cm}^{-3}$; Tra: $\epsilon_D''=0$; Inv: $N=5 \times 10^{18} \text{cm}^{-3}$; [0]: $\epsilon_M''=\epsilon_D''=0$)

To quantify the effect of the inverted carrier population on the behavior of the MD systems, we define the relative transmission enhancement factor (*TEF*) as

$$TEF \equiv T(5 \times 10^{18} \text{cm}^{-3}) / T(1 \times 10^{16} \text{cm}^{-3}), \quad (1)$$

the transmission under inversion with respect to transmission under absorption of the InGaAsP MQW. Figure 4(a) shows the *TEF* for the AZO-based multilayer at several different incident wavelengths. This system exhibits significant dispersion due to the proximity of the plasma frequency of AZO to the NIR. For shorter wavelengths, enhancement is negligible, indicating that realistic gain levels cannot compete with the strong damping at the plasmon resonance. As the wavelength increases to 1550nm, a modest *TEF* appears, increasing with the incident angle. However, this relative enhancement must be celebrated cautiously. The improvement in the *TEF* with increasing angle of incidence is offset by a drop in the absolute transmission of Fig. 3(a). Consequently, the overall effect of carrier inversion is quite small in the AZO/InGaAsP system.

Again, these results are best appreciated by contrasting to the Ag/InGaAsP system, the *TEF* of which is shown in Fig. 4(b). Relative enhancements close to a factor of 10 are observed over

the range of incident angles supported by this system, with several prominent peaks exceeding factors of 100 near the edges of the transmission window. In comparison to the AZO/InGaAsP system, the *TEF* has weak dispersion and is consistently larger in magnitude, indicating that the effect of the inversion in the Ag/InGaAsP system is much stronger.

Finally, the dependence of the average *TEF* on the number of periods for the Ag/InGaAsP system is shown in Fig. 4(c), where the *TEF* is averaged over the angular spectrum of the transmission window. The *TEF* is seen to increase exponentially with the length of the system. If the structure were used as an absorption modulator at a wavelength of 1500nm, for example, extinction ratios of 30dB were obtainable in a device length of just 2.1 μ m. Thus, if efficient coupling to this system is achieved, tunable and/or active, pump-dependent behavior may be feasible, enabling extremely compact and potentially electronically addressable optical amplifiers, sources, mixers, and modulators.

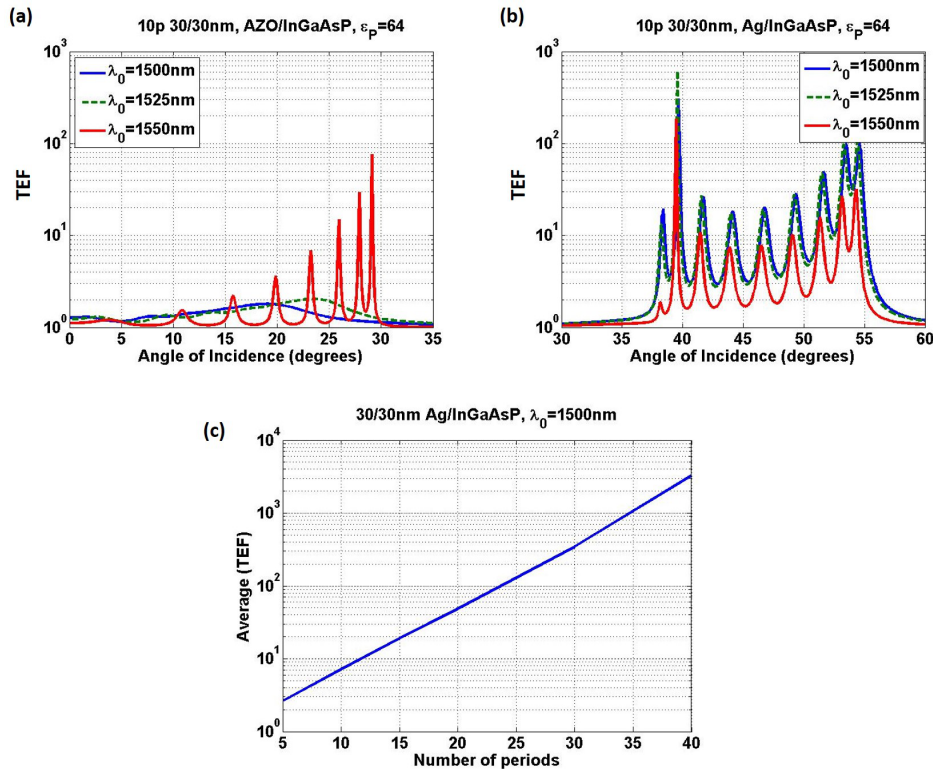


Fig. 4. Transmission enhancement factor (*TEF*) for TM-polarized light incident on 10-period (a) AZO/InGaAsP and (b) Ag/InGaAsP multilayer with 30nm layers, coupled via prism with $\epsilon_p=64$. (c) Angular-averaged *TEF* for the Ag/InGaAsP system with 30nm layers and wavelength of 1500nm as a function of number of periods.

4. Discussion

Prior work on gain-compensated plasmonic systems has emphasized that the Purcell effect has a deleterious role [28, 45]. Specifically, while the carrier densities required for significant improvement in transmission appear practically achievable, the required current densities may be extremely high [28]. This is a consequence of the large optical density of states in plasmonic and HMMs and the related high rates of spontaneous emission [52]. We stress, however,

that the Purcell effect in MD systems is most significant near the plasma frequency of the constituent metal and becomes less important as the frequency decreases. Using the expression [28] $F_P = 1 + \pi \Gamma k_{z,D} k_x \omega (dk_x/d\omega) / (\epsilon_D k_0)^3$ for the Purcell factor, F_P , at a single MD interface, where $k_{z,D}$ is the longitudinal wave-vector component in the dielectric, and ω and k_0 are the angular frequency and vacuum wave-number, respectively, we immediately notice that the Purcell enhancement in the AZO/InGaAsP system is significantly greater than unity due to the proximity of the AZO plasma frequency to the NIR (Appendix 1). On the other hand, the Purcell factor for the Ag/InGaAsP system is on the order of unity because $dk_x/d\omega \approx 0$ (Appendix 1). Therefore, while Purcell enhancement may cause the already stringent gain requirements for the AZO/InGaAsP system to increase, they may be considered a minor concern for the Ag/InGaAsP system.

To validate the SMM results on MD systems, we performed numerical FDTD simulations (Lumerical) of the transmission through a 10-period Ag/InGaAsP system with 30nm layers under the prism coupling configuration and with material parameters identical to the SMM. Periodic boundary conditions and perfectly matched layers (PML) were enforced in the transverse and longitudinal directions, respectively. For each simulation, the center wavelength, λ_C , of the finite-bandwidth pulse was tuned to match the wavelength of the monochromatic SMM calculations, λ_0 . Figures 5(a) and 5(b) compare transmission through this system at 1500nm and 1550nm, respectively, over a narrow angular range. The SMM is seen to consistently agree with FDTD results within a factor of two. Over the complete transmission window of the Ag/InGaAsP system, agreement between the SMM and FDTD worsens slightly, particularly at the second resonance of the transmission window (Appendix 2). The discrepancy between the SMM and FDTD results may be caused for several reasons, including imperfect PML, insufficient meshing, and the linewidth of the source. We provide FDTD simulation details in Appendix 2 and conclude that the finite-bandwidth of the FDTD source is the most likely reason for the discrepancy.

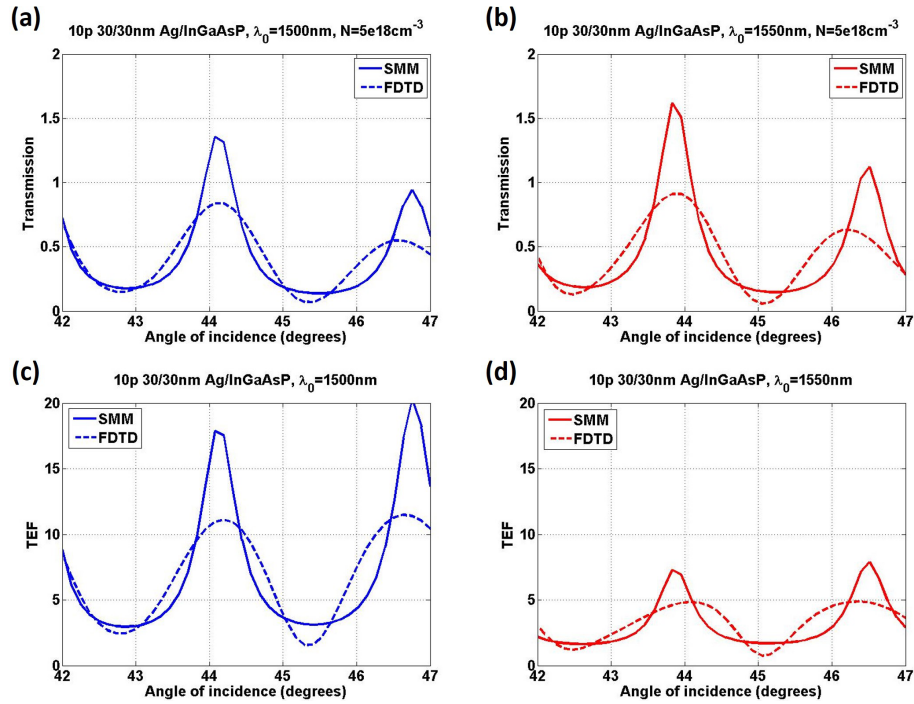


Fig. 5. (a,b) Transmission and (c,d) *TEF* through prism-coupled 10-period 30/30nm Ag/InGaAsP system under inversion at $\lambda_0 =$ (a,c) 1500nm and (b,d) 1550nm (SMM=scattering matrix method, FDTD=finite-difference time-domain).

The close, but albeit non-exact, agreement between the SMM and FDTD in the static case suggests that FDTD may be useful for studying the dynamics of periodic MD systems with loss and gain. Throughout this analysis we have assumed a steady-state gain model, which implies continuous wave external pumping conditions. A logical extension of the present work is therefore an FDTD study incorporating spatial dependence of the gain within each semiconductor layer, as well as the use of a self-consistent gain model that takes into account transient and nonlinear effects [53, 54]. The inhomogeneously broadened lineshape of InGaAsP MQWs however poses challenges in this regard, as a simple 4-level system [55] does not capture the electronic density of states responsible for the broadening. A potential solution to this problem is the use of a superposition of 4-level systems, each with a slightly different transition frequency. The added accuracy of this approach, however, would come at the expense of large memory and processing requirements. Nonetheless, the utility of the FDTD method in studying transient and nonlinear effects is one of our motivations for comparing SMM and FDTD results under steady-state conditions.

5. Conclusion

We have analyzed transmission of high- k waves in the presence of loss and gain through metal-InGaAsP systems. We have shown that, under moderate pumping, Ag/InGaAsP may support transmission of high- k modes enhanced by several orders of magnitude, relative to the unpumped case, and absolute transmission on the order of unity. While the magnitude of the enhancement factor for the AZO/InGaAsP system is significant, the absolute transmission is rather negligible. We have further shown that the Purcell effect does not have a strong deleteri-

ous role for the Ag/InGaAsP system. Finally, we have compared results based on the SMM with numerical FDTD simulations. The results provide a rigorous foundation for further theoretical work on the nonlinear dynamics of multilayer MD systems based on InGaAsP MQWs and justification for experimental efforts to circumvent the confinement-loss tradeoff fundamental to plasmonic and hyperbolic metamaterials.

Appendix 1: Use of Bloch's Theorem and the TMM in analysis of MD systems

To date, most work on the analysis of MD systems and HMMs has relied upon the transfer matrix method (TMM). For example, greater-than unity transmission through Ag/TiO₂ multilayers was predicted via TMM by Cortes et al [52]. This result is unphysical because loss and gain were omitted. In the presence of loss and gain, Savelev et al. used the TMM method to analyze transmission through Ag/PMMA systems [45]. While the reported transmission is plausible, no attempt was made to validate the results with numerical methods.

In addition to transmission, the TMM is routinely used to calculate the complex amplitude reflectivity of HMMs, upon which the photonic density of states and emission lifetimes are often calculated. This was done, for example, by Galfsky et al. on quantum dots in Ag/Al₂O₃ multilayers [14], by Lu et al. and Ferrari et al. on dyes in Ag/Si systems [12,56], and by Cortes et al. for Ag/TiO₂ [52]. The TMM was also used to elucidate the presence of volume plasmon polaritons in Au/Al₂O₃ multilayers by Zhukovsky et al. [52], and to calculate the bandstructure of HMMs in the presence of gain [57].

While useful qualitatively, the TMM is known to become increasingly numerically unstable as the structure increases in length [46], as strong loss or gain is incorporated [48], and as evanescent modes are considered [58]. The essential difference between the TMM and SMM lies in the fact that the matrices of the former contain exponential functions with arguments of different sign [46–48, 58, 59]. For large propagation lengths or large values of the imaginary component of the wave-vector, one of the exponentials will diverge. The matrices of the SMM on the other hand contain exponentials with arguments of the same sign, which prevent the instabilities that limit the utility of the TMM. Given these facts, it is imperative to use a more stable method for calculating absolute transmission of high-*k* modes in the presence of loss and gain, as well as relative transmission enhancement.

Nevertheless, the TMM does correctly predict the bounds to the transmission resonances in *k*-space. Because it is simpler to implement than the SMM, it is useful for studying the dispersion of MD systems. Figure 6 shows transmission contours with loss and gain omitted calculated via TMM with explicitly evanescent fields for 10-period 30/30nm MD systems. Qualitatively, we observe that the AZO/InGaAsP system of Fig. 6(a) exhibits little dispersion ($d\lambda_0/dk_x \approx 0$), while the Ag/InGaAsP system of Fig. 6(b) is highly dispersive ($d\lambda_0/dk_x \gg 0$). This is a direct consequence of the fact that the plasma frequencies of AZO and Ag lie within and outside the NIR, respectively. The greater-than-unity transmission in the absence of gain is a quantitatively unphysical result and motivates the use of the SMM for absolute transmission and relative transmission enhancement calculations.

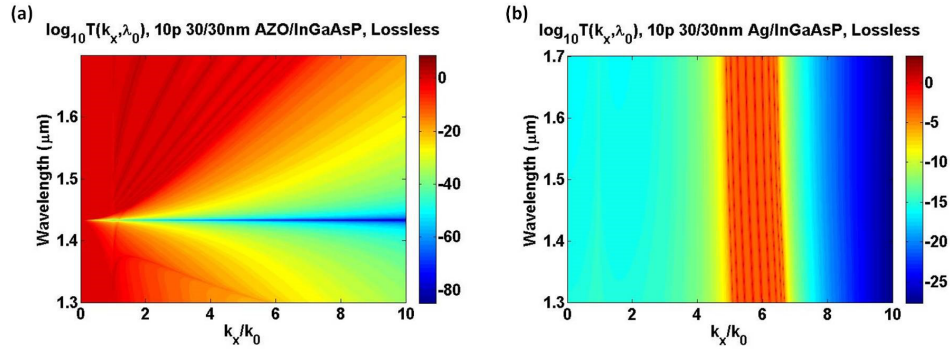


Fig. 6. Transmission as a function of wavelength and in-plane wavenumber for 10-period 30/30nm (a) AZO/InGaAsP and (b) Ag/InGaAsP systems with losses and gain omitted. The greater-than-unity transmission in the absence of gain is an unphysical result that motivates the use of the SMM.

Appendix 2: Discrepancy between SMM and FDTD

The discrepancy in absolute transmission between the SMM and FDTD calculations is almost negligible at the high- k end of the transmission window, but becomes significant at small values of k_x , in particular at the second angular resonance of Fig. 7(a), which is calculated at an angular resolution of 7 samples per degree. Potential reasons for this discrepancy include FDTD errors caused by imperfect PMLs, insufficiently small mesh size, and the finite bandwidth of the source. The bandwidth of the plane wave source used in the FDTD simulations was 200nm at a center wavelength of 1500nm or 1550nm. The timestep Δt was 0.00310473 fs, and was determined by the spatial step Δz and meeting the stability criterion that $c\Delta t/\Delta z < 1$, where c is the speed of light in vacuum. In all of the simulations we used 100 mesh cells per wavelength with a minimum mesh step of 0.1 nm and a grading factor of 1.41421. Bloch boundary conditions were used in the direction parallel to the layer interfaces and uniaxial anisotropic PML were used in the direction normal to the layer interfaces. The PML was polynomial order 3 and consisted of 12 layers with $\kappa=2$, $\sigma=0.25$, and α undefined, where κ , σ , and α are parameters for expressing Maxwells Equations in stretched-coordinate form [60].

Generally, PMLs are optimized to function at normal incidence and are known to produce unwanted reflections for broadband sources at oblique incidence, particularly for non-center frequencies [60]. To test this potential problem, we increased the PML thickness from 12 layers to 40 layers. However, we found negligible change in the transmission spectra. To test potential meshing errors, we reduced the mesh size from the default minimum of 4nm to 0.1nm in both the direction normal and parallel to the layer interfaces, but also found negligible change in transmission.

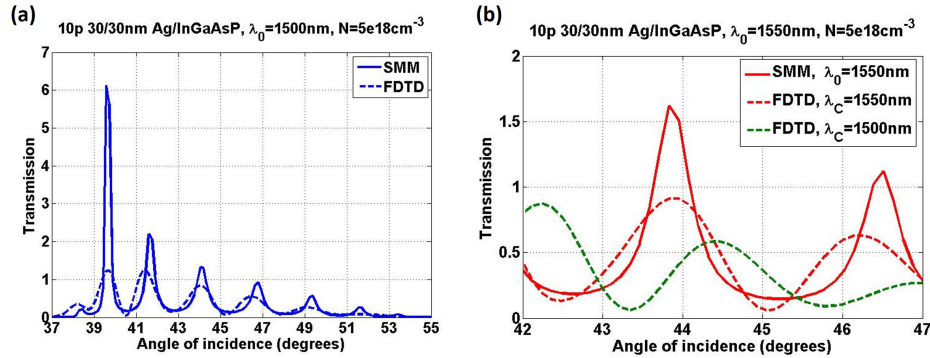


Fig. 7. Transmission through prism-coupled 10-period 30/30nm Ag/InGaAsP system under inversion at (a) $\lambda_0=1500\text{nm}$ and (b) $\lambda_0=1550\text{nm}$ (SMM=scattering matrix method, FDTD=finite-difference time-domain). In (b) the center wavelength, λ_C , used for the FDTD source is varied from 1500nm to 1550nm to show that results between SMM and FDTD most closely match for $\lambda_0 = \lambda_C$.

We did however find that the transmission spectra between SMM and FDTD most closely match when the center wavelength, λ_C , of the FDTD source coincides with the wavelength of the monochromatic SMM source. Figure 7(b) shows transmission spectra through the same Ag/InGaAsP multilayer at $\lambda_0=1550\text{nm}$, calculated by the SMM and with broadband FDTD sources having center wavelengths of 1500nm and 1550nm. The discrepancy between the SMM and FDTD result increases as the center wavelength deviates from 1550nm, suggesting that the finite bandwidth of the FDTD source, relative to the monochromatic SMM source, is the most plausible cause for the general discrepancy between the SMM and FDTD results. Potential problems with FDTD simulations involving gain media also include convective and absolute instabilities [61], though these do not hamper our simulation results because we have assumed pumping levels to achieve carrier densities only a factor of two above the transparency condition [40].

Acknowledgments

The authors wish to thank Prof. Antione Moreau for helpful discussions. This work was supported by the Office of Naval Research Multidisciplinary Research Initiative (N00014-13-1-0678), the National Science Foundation (NSF) (ECE3972 and ECCS-1229677), the NSF Center for Integrated Access Networks (EEC-0812072, Sub 502629), the Defense Advanced Research Projects Agency (N66001-12-1-4205), and the Cymer Corporation.